ELSEVIER

Promoted Ru–hydroxyapatite: designed structure for the fast and highly selective oxidation of alcohols with oxygen

Z. Opre, J.-D. Grunwaldt, M. Maciejewski, D. Ferri, T. Mallat, A. Baiker *

Department of Chemistry and Applied Biosciences, Swiss Federal Institute of Technology, ETH Hönggerberg, CH-8093 Zürich, Switzerland

Abstract

Ru-containing hydroxyapatite (HAp) catalysts have been developed for the oxidation of alcohols with molecular oxygen in an organic solvent. The working hypothesis has been that fine-tuning of the location and surroundings of the active Ru species would provide outstanding performance. The highest oxidation activity was achieved when (i) the contact time between the metal salt solution and HAp was limited to a few minutes to minimize restructuring via dissolution–redeposition, (ii) low Ru content was applied, (iii) Co^{2+} and Pb^{2+} promoters were incorporated to occupy the poorly accessible "hidden" sites in HAp before the introduction of Ru^{3+}, thus facilitating egg-shell-type Ru distribution in the particles, and (iv) after Ru incorporation the catalysts were dried at moderate temperature to avoid restructuring induced by dehydration of the active sites and their neighborhood. It is assumed that the active sites are $Ru(OH)^{2+}$ species stabilized by the phosphate O atoms and adsorbed (H-bonded) water. Various methods have been used for characterization of these catalysts, including XPS, DRIFT spectroscopy, inductively coupled plasma optical emission spectroscopy (ICP-OES), XRD, thermogravimetry combined with mass spectroscopy (pulse thermal analysis), and nitrogen adsorption. One of the two best catalysts (RuCoHAp-10min) was used in the partial oxidation of benzylic, allylic, aliphatic and cycloaliphatic alcohols. Most carbonyl compounds were produced in excellent yields without the formation of any detectable by-product. The catalytic activity seems to be higher than that of other Ru-based solid catalysts developed for the aerobic oxidation of alcohols.

© 2004 Elsevier Inc. All rights reserved.

Keywords: Promoted Ru–hydroxyapatite; Aerobic oxidation; Alcohols; Ru–Co–hydroxyapatite; Ru–Pb–hydroxyapatite

1. Introduction

The transformation of alcohols into carbonyl compounds is an important reaction in organic synthesis. From environmental and technical points of view, an attractive solution is the application of a heterogeneous catalyst and molecular oxygen as the sole oxidant (Scheme 1) [1–6]. There has been a growing interest in recent years in the application of ruthenium-based solid catalysts [7], including $RuO_2 \cdot x H_2O$ [8], RuO_2/FAU zeolite [9], Ru/Al_2O_3 [10], Ru–Al–Mg–hydrotalcite [11], Ru–silicotungstate [12], and Ru–hydroxyapatite (RuHAp) [13]. Their activity is mod-
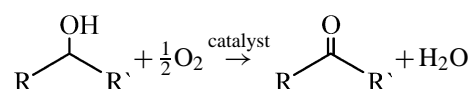
R,R′: H, alkyl, cycloalkyl, allyl, aryl

Scheme 1. Oxidation of alcohols to aldehydes and ketones.

erate compared with some platinum- and palladium-based catalysts, but the selectivity for the aldehyde intermediate is usually high in the oxidation of a wide range of activated and nonactivated alcohols.

Stoichiometric calcium hydroxyapatite, $Ca_{10}(PO_4)_6(OH)_2$ (CaHAp), has a hexagonal structure constructed from columns of calcium ions and oxygen atoms that are located parallel to the hexagonal axis [14–16]. Three oxygen atoms

of each PO_4 tetrahedron are shared by one column, and the fourth oxygen atom is attached to a neighboring column. The crystal structure presents two nonequivalent Ca sites. Site I contains Ca^{2+} ions in a columnar arrangement, and each Ca^{2+} ion is coordinated to nine oxygen atoms proceeding from phosphates. Calcium cations at site II are hepta-coordinated by six oxygen atoms belonging to five PO_4^{3-} anions and one OH^- anion. These Ca^{2+} ions at site II are in equilateral triangles centered on the screw axes. The OH^- ions are too large to fit into the triangles of Ca^{2+} ions at site II; they occupy disordered positions above or below the Ca triangles.

The Ca^{2+} ions in the lattice can be exchanged with other cations. If the charge of the substituting cation is different from that of Ca^{2+} ions, the charge compensation mechanism may have a big influence on the apatite structure. Large divalent cations (e.g., Pb^{2+}) replace Ca^{2+} at Ca II sites, whereas small divalent cations (e.g., Zn^{2+}) replace Ca^{2+} at Ca I sites [17]. Some small cations such as Ni^{2+} and Co^{2+} can replace Ca^{2+} at Ca II sites, resulting in a destabilizing effect on the apatite structure [18]. The following mechanisms have been proposed for the replacement of Ca^{2+} ions in HAp by other metal ions: ion exchange, ion adsorption, dissolution of HAp followed by deposition of a new phase, and a combination of these possibilities [19].

Hydroxyapatite-based materials have been applied as catalysts in various transformations, including oxidation [20–22], dehydrogenation [23], dehydration [24], epoxidation [25], removal (deprotection) of *N*-benzyloxycarbonyl groups [26], racemization of alcohols [27], Knoevenagel condensation [28], and Diels–Alder and aldol reactions [29]. Yamaguchi et al. [13] reported the first application of apatite-based catalysts in the partial oxidation of alcohols in the liquid phase, with molecular oxygen as an oxidant. The 17 wt% Ru-HAp catalyst was prepared by ion exchange of stoichiometric hydroxyapatite (HAp) with an aqueous $RuCl_3$ solution for an extended period of 24 h.

A basic limitation of HAp as a catalytic material is the location of the majority of Ca^{2+} ions in the narrow, zeolite-like channels of the lattice [22]. This situation is particularly detrimental in liquid-phase reactions at close to ambient conditions because of the low diffusion rates. Here we report a new approach to improving the catalytic performance of Ru-exchanged HAp. We assumed that the preferential location of the isolated Ru species at or close to the surface of the HAp particles should improve the activity compared with the original RuHAp catalyst developed by Yamaguchi et al. [13]. To achieve this goal, metal promoters were added to occupy the "hidden" sites inside the narrow channels, the total amount of ruthenium was reduced, a short contact time was used for the introduction of Ru, and the usual catalyst pretreatment temperature was lowered to minimize dehydration and restructuring of the metal-exchanged apatite.

2. Experimental

2.1. Materials

Starting materials for catalyst preparation were $RuCl_3$ hydrate (36% Ru, 99.9%; ABCR), aqueous ammonia solution (ca. 25% NH_3; Merck), $(NH_4)_2HPO_4$ (98%; ABCR), $Ca(NO_3)_2 \cdot 4H_2O$ (99%; Strem Chemicals), $CoCl_2 \cdot 6H_2O$ (99.9%; Acros), $FeCl_3 \cdot 6H_2O$ (99.9%; Acros), $NiCl_2 \cdot 6H_2O$ (99.9%; Acros), and $Pb(CH_3COO)_2 \cdot 3H_2O$ (99.5%; Merck). Benzyl alcohol (> 99%; Fluka), 2-adamantanol (> 98%; Fluka), 2-thiophenemethanol (> 99%; Acros), 4-nitrobenzyl alcohol (99%; Acros), 2-octanol (> 99.5%; Fluka), geraniol (99%; Acros), 4-chlorobenzyl alcohol (99%; Acros), 1-phenylethanol (98%; Aldrich), cinnamyl alcohol (97%; Fluka), 1-octanol (99.5%; Fluka), 2-(hydroxymethyl)pyridine (98%; Acros), 4-methoxybenzyl alcohol (> 98%; Fluka), 4-methylbenzyl alcohol (98%; Acros), and mesitylene (99%; Acros) were used as received.

2.2. Catalyst preparation

The abbreviations of the catalysts used throughout this paper can be explained with the example of a Co-promoted Ru–hydroxyapatite, "RuCoHAp-24h." "Ru" and "Co" indicate that the Ca^{2+} ions in hydroxyapatite (HAp) have been partially replaced at first with Co^{2+} ions and then with Ru^{3+} ions. The time at the end of the abbreviation ("10min" or "24h") indicates the contact time of the $RuCl_3$ solution with HAp.

Stoichiometric calcium hydroxyapatite $Ca_{10}(PO_4)_6(OH)_2$ (HAp) was synthesized by a wet chemical method according to a known procedure and calcined at 500 °C for 3 h [30]. Next, we introduced the promoter metal by shaking 1.0 g HAp with 75 ml of a 6.7 mM aqueous solution of $CoCl_2$ for 20 min or with 75 ml of 6.7 mM aqueous solution of $Pb(CH_3COO)_2$, $FeCl_3$, or $NiCl_2$ for 24 h. The solid (CoHAp, PbHAp, FeHAp, or NiHAp) was filtered off and washed with deionized water. We introduced ruthenium by shaking the wet material with 75 ml of a 6.7 mM aqueous $RuCl_3$ solution at room temperature for 10 min or 24 h. The RuCoHAp, RuPbHAp, RuFeHAp, or RuNiHAp catalyst was filtered off, washed with deionized water, and dried for 8 h at 80 °C in vacuum. We synthesized the RuHAp catalyst without promoter metal analogously, by shaking HAp with the aqueous $RuCl_3$ solution. Portions of the RuHAp and RuCoHAp catalysts were dried at different temperatures (25, 80, 110, and 180 °C) in vacuum to investigate their thermal stability.

2.3. Structural evolution of metal-exchanged hydroxyapatite

HAp (2.0 g) in 150 ml of a 6.7 mM aqueous solution of $RuCl_3$ or $CoCl_2$ was shaken for 24 h or for 20 min. In the latter case the Co-exchanged solid (CoHAp) was filtered off and washed with deionized water, and then shaken in 150 ml

of a 6.7 mM aqueous solution of $RuCl_3$ at room temperature for 24 h. The pH of the solutions was monitored with a glass electrode. For each sample, 10 ml of the well-mixed slurry was collected occasionally with a syringe and the solid was filtered off immediately. The Ca, Co, Ru, and P concentrations in the filtrate and the metal/P ratio of the solid (after dissolution in diluted HCl) were determined by inductively coupled plasma optical emission spectroscopy (ICP-OES).

2.4. Characterization techniques

The BET surface area and pore size distribution were determined by N_2 adsorption–desorption at 77 K with a Micromeritics ASAP 2010 instrument. Before measurement the samples were degassed in vacuum at 150 °C.

X-ray powder diffraction (XRD) analysis was carried out with a Siemens D5000 powder X-ray diffractometer and Cu-K_α radiation in the step scanning mode between 20° and 80° (2θ), with a step size of 0.01° and 2 s/step.

Thermogravimetry (TG) combined with mass spectrometry (MS) was carried out with a Netzsch STA 409 thermoanalyzer, which was connected to a valve device enabling pulse thermal analysis (PulseTA) [31]. This setup allowed the injection of controlled amounts of probe gas into an inert carrier gas stream (He) flowing through the thermoanalyzer. The composition of the gas phase was monitored with a Balzers QMG 420 quadrupole mass spectrometer, which was connected to the thermoanalyzer by a heated (ca. 200 °C) stainless-steel capillary.

The typical procedure of the TG-MS redox experiment was as follows. At first the catalyst was heated in a He flow to the specific pretreatment temperature (80, 150 °C) to remove water. We tested the redox properties by injecting pulses of H_2 at this temperature into He carrier gas, followed by O_2 pulses (PulseTA).

X-ray photoelectron spectroscopy (XPS) analysis was performed on a Leybold Heraeus LHS 11 MCD instrument (analysis chamber) containing an X-ray source RQ 20/38 (Specs), with Al-K_α radiation (1486.6 eV). The sample was pressed into a sample holder, evacuated in a load lock to 10^{-6} mbar, and transferred to the analysis chamber (typical pressure $< 10^{-9}$ mbar) [32].

Because of the overlap of the C $1s$ and Ru $3d_{3/2}$ and Ru $3d_{5/2}$ peaks and the small intensity of the C $1s$ peak, the peaks were energy-shifted to the binding energy of P $2p$ (132.9 eV) to correct for the charging of the material. For quantification of the composition the following peaks were used: O $1s$, P $2p$, Cl $2p$, Co $2p$, Ru $3p_{3/2}$, Ca $2p$, Fe $2p$, Ni $2p$, and Pb $4f$. The energy correction, background subtraction, and quantification of the surface concentration were performed with the SPECSLAB software package. Sensitivity factors used for the calculation of catalyst surface composition were taken from Wagner et al. [33].

Diffuse reflectance infrared (DRIFT) spectra were collected with a Bruker Optics Equinox-55 by co-addition of 100 scans at 4 cm^{-1} resolution. The instrument was equipped with a HVC-DRP2 reaction chamber (Harrick) and a liquid nitrogen-cooled MCT detector. Samples were diluted with KBr, and reference spectra of KBr were acquired at different temperatures according to the same procedures as used for the samples.

2.5. Alcohol oxidation

The slurry containing the catalyst and alcohol in toluene was stirred in a 50-ml glass reactor at 60 or 90 °C, in the presence of oxygen at 1 bar. After reaction the catalyst was filtered off and washed carefully with 2-propanol. The selectivity and conversion were determined by GC analysis (Thermo Quest Trace 2000, equipped with an HP-FFAP capillary column and FID detector), with mesitylene as internal standard, and the products were identified by authentic samples. The reaction rate was characterized by the average TOF at high conversion: TOF = [mol(alcohol)/mol(Ru)]/h.

Note that toluene forms an explosive mixture with air in the range of ca. 1–8 vol% toluene [34]. Thus, oxidation at temperatures close to the boiling point of toluene is less dangerous.

3. Results and discussion

3.1. Chemical processes during the evolution of metal-exchanged hydroxyapatite

The processes occurring during the introduction of Ru^{3+} and Co^{2+} ions into HAp have been followed by ICP-OES analysis of the aqueous solution. The disappearance of Ru from the solution was rapid, and in a parallel process HAp leached considerably (Fig. 1A). After about 1 h the concentrations of Ca and P in solution reached steady values, and 99.9% of Ru entered the solid phase within 3 h. During these processes the pH of the solution increased significantly (Fig. 1B).

Incorporation of Co into HAp was remarkably faster (Fig. 2A) than that of Ru. The Co concentration in the aqueous solution did not change after 5 min, in agreement with earlier observations [35]. Dissolution of Ca and P from HAp was less extensive than in the case of Ru incorporation, and the pH changed in the opposite direction (Fig. 2B).

Interaction of CoHAp with the $RuCl_3$ solution is illustrated in Fig. 3. In addition to leaching of Ca and P, Co dissolution was also detected at the beginning of the interaction. One-third of the total Co went into solution in 10 min, and this ratio decreased slowly to 24% after 24 h.

Interpretation of these data is not straightforward. The real nature of the interaction between hydroxyapatite and metal ions in aqueous solution is still debated. Three types of mechanisms have been proposed: surface adsorption, ion exchange between Ca^{2+} and metal ions involving diffusion into the solid, and dissolution of HAp and precipitation of a new phase (or phases) [19,36–38]. These processes often
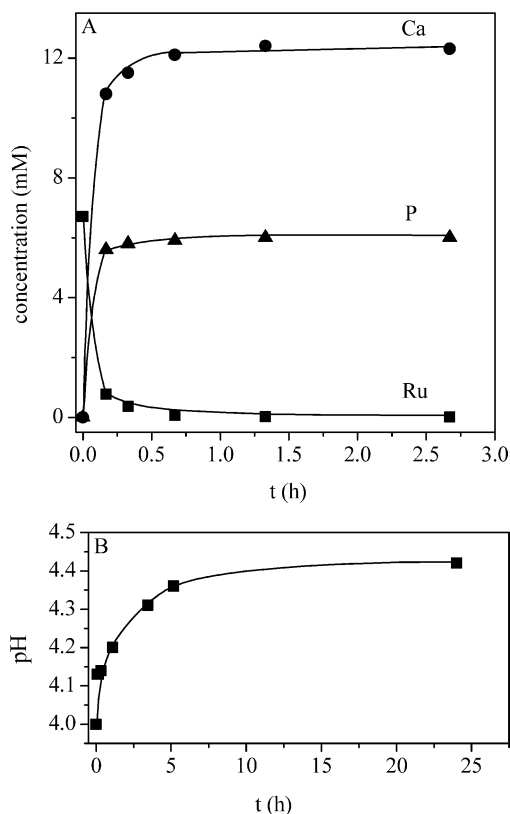
Fig. 1. Variation of the concentration of ruthenium, calcium and phosphorous (A), and the shift of pH (B) in solution during interaction of an aqueous RuCl₃ solution with calcined hydroxyapatite (HAp).

act together, and it is hard to prove the dominance of one process.

Obviously, adsorption of Ru^{3+} or Co^{2+} ions (and Cl^{-} ions) on the apatite surface is the first step that is inevitable, even if ion-exchange or dissolution–precipitation becomes dominant in the second stage of the interaction. In the case of Ru introduction the initial pH of the aqueous RuCl₃ solution was only 4.0, and this relatively low pH facilitates dissolution of HAp [19,38]. Note that the initial pH could not be increased without deposition of a fraction of Ru. Dissolution of HAp [Eq. (1)] is indicated by the presence of P in solution and the excess of dissolved Ca related to Ru incorporated.

$$Ca_{10}(PO_4)_6(OH)_2 + 14H^+ \rightarrow 10Ca^{2+} + 6H_2PO_4^- + 2H_2O. \tag{1}$$
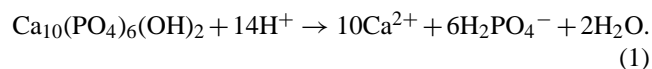
Dissolution of HAp is also significant during the introduction of Co, though to a lower extent than in the case of Ru incorporation. The difference is attributed mainly to the different pH of the starting solutions (Figs. 1–3).

3.2. Catalyst composition by ICP-OES and XPS analysis

The bulk composition of the Ru-containing catalysts is summarized in Table 1. Elemental analysis by ICP-OES indicated that the Ca/P ratio in HAp corresponded to the theoretical value of stoichiometric hydroxyapatite (1.67) [30].
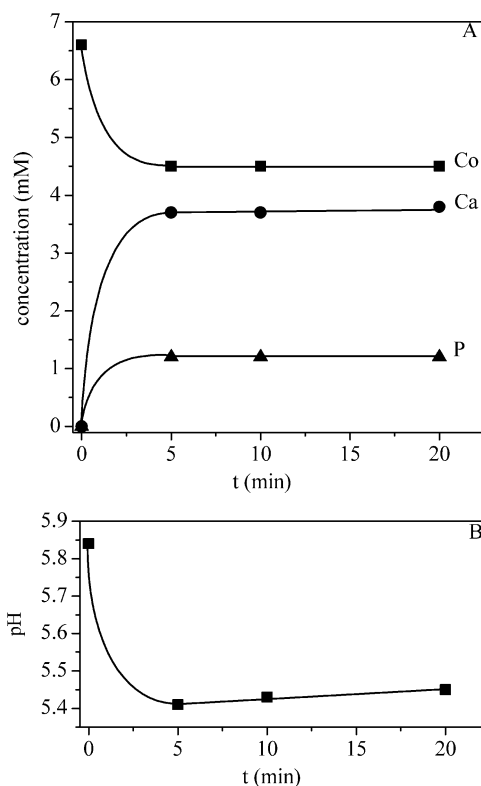

Fig. 2. Time-dependent changes in the concentrations of cobalt, calcium and phosphorous (A), and that of pH (B) in solution during interaction of an aqueous CoCl₂ solution with calcined hydroxyapatite (HAp).
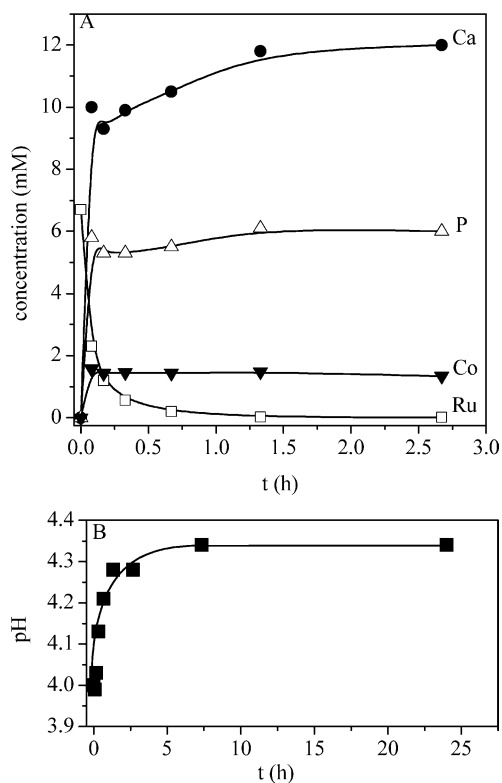

Fig. 3. Changes of the concentration of ruthenium, cobalt, calcium and phosphorous (A), and variation of the pH (B) in solution during interaction of RuCl₃ in an aqueous solution with CoHAp.

Table 1

Bulk composition of the catalysts determined by ICP-OES. X indicates the promoter cation (Co^{2+}, Fe^{3+}, Ni^{2+}, or Pb^{2+})

Catalyst	Ca/P	(Ru + X + Ca)/P	(Ru + X)/Ca	Ru/Ca	X/Ru	Ru (wt%)	X (wt%)
RuHAp-24h	1.45	1.51	0.045	0.045	–	4.0	–
RuHAp-10min	1.60	1.66	0.040	0.040	–	3.8	–
RuCoHAp-24h	1.42	1.51	0.059	0.040	0.47	3.5	1.0
RuCoHAp-10min	1.60	1.67	0.046	0.036	0.26	3.4	0.5
RuFeHAp-24h	1.51	1.67	0.110	0.055	1.06	4.1	2.8
RuNiHAp-24h	1.61	1.69	0.047	0.036	0.31	3.4	0.6
RuPbHAp-24h	1.55	1.71	0.095	0.039	1.23	4.1	10

All ratios are calculated as molar ratios.

Table 2

Surface composition of the catalysts measured with XPS

Catalyst	Ru $3p_{3/2}$ (mol%)	X (mol%)	P $2p$ (mol%)	Ca $2p$ (mol%)	O $1s$ (mol%)	Cl $2p$ (mol%)	Ru/Ca	(Ru + X)/Ca	X/Ru
RuHAp-24h	5.1	–	9.6	12.9	72.3	0	0.39	0.39	–
RuHAp-10min	4.2	–	9.3	14.2	71.9	0.4	0.29	0.29	–
RuCoHAp-24h	3.6	1.4	9.0	14.0	71.1	0	0.26	0.36	0.39
RuCoHAp-10min	4.7	1.8	8.6	13.4	70.4	0.5	0.35	0.48	0.38
RuFeHAp-24h	5.3	5.2	8.6	10.3	70.5	0.1	0.51	1.02	0.98
RuNiHAp-24h	4.3	0.7	9.4	14.1	71.4	0	0.30	0.35	0.16
RuPbHAp-24h	5.7	3.8	6.5	9.9	73.4	0.4	0.58	0.96	0.67

X indicates the promoter cation (Co^{2+}, Fe^{3+}, Ni^{2+}, or Pb^{2+}). All ratios are calculated as molar ratios.

In the Ru-containing catalysts the (Ca + Co + Ru)/P ratio did not change significantly, except when a prolonged contact time of 24 h was used for introducing Ru. In these cases the total metal/P ratio decreased by up to 10% (to 1.51). In a control experiment we applied a higher $RuCl_3$ concentration, as suggested by Yamaguchi et al. [13], and the expected value of 1.67 could be reproduced even after a 24-h contact time. A possible explanation for this discrepancy is that the mechanism of introducing metal ions into HAp and thus the structure of the catalyst depend on the experimental conditions.

Importantly, according to ICP-OES analysis none of the RuHAp catalysts contained Cl^- ions (< 72 ppm Cl). Similarly, XPS analysis indicated only trace amounts of Cl on the surface of some catalysts (Table 2), likely because of incomplete washing of the samples. This observation is in contrast to the former report of Yamaguchi and co-workers [13], who found that the Ru:Cl ratio on the surface of the 17 wt% RuHAp was 1:1, corresponding to an active species of $RuCl^{2+}$. Note that Wuyts et al. were also unable to detect Cl by XPS in their RuHAp catalysts containing 0.5 or 2 wt% Ru [27].

The moderate increase in the total Ru content in RuHAp with increasing contact time (Table 1) is in agreement with the analysis of the aqueous solutions shown in Fig. 1. A comparison of the bulk and surface Ru/Ca ratios in Tables 1 and 2 reveals a remarkable surface enrichment of Ru.

Tables 1 and 2 list ICP-OES and XPS data for the promoted catalysts. The total amount of incorporated Ru remained in a narrow range of 3.4–4.0 wt% for all catalysts. In contrast, the promoter metal content in the bulk varied between 0.5 wt% (Co) and 10 wt% (Pb), despite of the identical conditions applied in catalyst preparation. A comparison of the surface and bulk Ru/Ca ratios reveals that both the contact time and the presence of promoter influence the distribution of Ru ions in the final catalyst. Note the outstanding characteristics of RuPbHAp: this catalyst contains the highest total amount of promoter, which apparently leads to the highest surface enrichment of Ru.

The binding energy (BE) of Ru in RuHAp did not change with the contact time between HAp and the $RuCl_3$ solution (Table 3), but it decreased with a longer contact time in the presence of Co in the catalyst (Fig. 4). The probable explanation for the decrease in the BE of Ru in RuCoHAp-24h is the change in the coordination ("ligand sphere") of Ru^{3+} ions in the catalyst with time due to catalyst restructuring during the prolonged contact time. Note the decrease in the BE of Ru between $RuO_2 \cdot H_2O$ (282.5 eV) and RuO_2 (280.7 eV) [39]. Hence, aggregation of Ru species on the surface after 24 h may lead to such a decrease in BE.

The BEs of the metal ions were investigated by XPS analysis to study the synergetic effect of promoter metals. The BE of the phosphorous $2p$ (132.9 eV) was taken as the reference. The data are collected in Table 3. The BEs of Ca and P did not change in the different samples (Ca $2p_{3/2}$: 346.9 eV, Ca $2p_{1/2}$: 350.5 eV and P $2s$: 190.2 eV). The Ru $3d_{5/2}$ signal was observed in the RuHAp samples at 282 eV. Wuyts et al. analyzed 0.4 and 1.31 wt% RuHAp catalysts and reported a BE of 281.3 eV (they took the BE of the carbon $1s$ as the reference at 284.9 eV), and the oxidation state of ruthenium was found to be Ru^{3+} by EPR spectroscopy [27]. This difference might result from the higher Ru content (4 and 3.8 wt%) and the different environment of the Ru^{3+} ions in our samples. A similar observation was described for

Table 3
Binding energies (BE) of Ru, Co, Fe, Ni, Pb and O in different catalyst samples measured by XPS

Catalyst	BE (eV) of promoter				BE (eV) of Ru				BE (eV) of O
	Co				$3p_{3/2}$	$3p_{1/2}$	$3d_{5/2}$	$3d_{3/2}$	$1s$
	$2p_{3/2}$		$2p_{1/2}$						
RuHAp-24h					463.4	485.5	282	286.1	530.6
RuHAp-10min					463.5	485.6	282.1	286.1	530.8
RuCoHAp-24h	781.7	787.1	797.2	802.7	462.6	485.6	281.1	285.1	530.9
RuCoHAp-10min	781.95	786.47	797.17	803.1	463.3	485.6	282	286	530.7
	Fe								
RuFeHAp-24h	711.7		725.4		463.7	486.1	282.2	286.1	530.6
	Ni								
RuNiHAp-24h	856.1	861	873.5	878.3	462.6	485	281.2	285.1	530.7
	Pb								
	$4f_{7/2}$	$4f_{5/2}$	$4d_{5/2}$						
RuPbHAp-24h	138.2	143.1	413.4		463.4	485.8	282.1	285.9	530.7
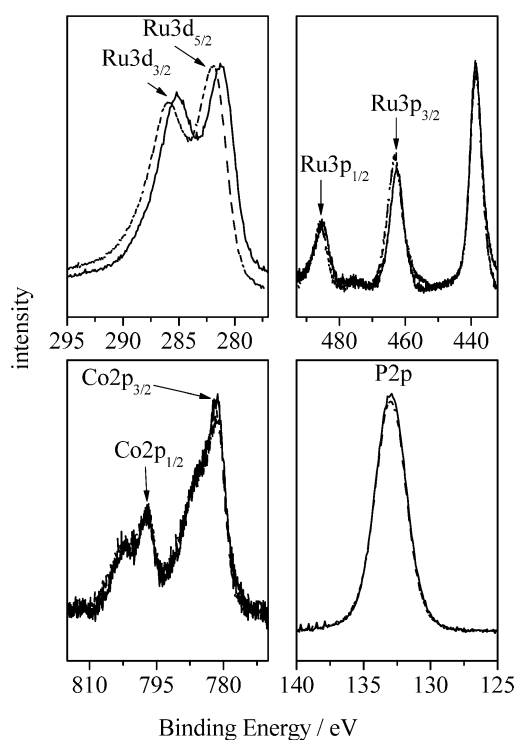
Fig. 4. XP spectra of RuCoHAp-24h (continuous line) and RuCo-HAp-10min (dashed line); all spectra are corrected for charging with respect to P $2p$.

FeHAp [40], where the BE of Fe $2p_{3/2}$ was dependent on the Fe content. The BE of the Ru $3d_{5/2}$ did not change in RuFeHAp-24h and RuPbHAp-24h compared with RuHAp-24h, but it decreased in RuCoHAp-24h and RuNiHAp-24h.

The Co $2p_{3/2}$ BE in RuCoHAp-10min and RuCoHAp-24h catalysts (Table 3) is in the range characteristic for Co^{2+} (781–783 eV) [41,42]. The Co $2p$ spectrum shows a strong shake-up peak, which is also characteristic for Co^{2+}. The spin-orbital splitting, however, indicates the presence of some Co^{3+} on the surface (15.2–15.5 eV) [22].

The peak for Fe $2p_{3/2}$ in RuFeHAp-24h appears at 711.7 eV (Table 3). This value is close to the BE of Fe in FeOOH (711.9 eV) [40], where the Fe^{3+} ions are coordinated by O atoms and OH^- ions. Ishikawa et al. [40] found that the peak for Fe $2p_{3/2}$ appears at 711.5 and 712.1 eV for FeHAp at $X(Fe) = 0.06$ and 0.11, where $X(Fe)$ represents the surface concentration of Fe^{3+} related to the sum of the surface concentrations of Fe^{3+} and Ca^{2+}. The latter value is more similar to that in our sample, where $X(Fe) = 0.18$, considering the Ca $2p_{3/2}$ in their sample (347.5 eV) and in our sample (346.9 eV).

The Pb $4f_{7/2}$ BE in RuPbHAp-24h is at 138.2 eV (Table 3), which is close to the BE of Pb in $Pb_3(PO_4)_2$ (138.6 eV), $Pb(OH)_2$ (138.4 eV), and PbO (137.9 eV) [43,44].

The BEs of Ni $2p_{3/2}$ and $2p_{1/2}$ in RuNiHAp-24h are at 856.1 and 873.5 eV, and the shake-up satellites are at 861 and 878.3 eV (Table 3). The BE of Ni $2p_{3/2}$ in RuNiHAp-24h is close to that in $Ni(OH)_2$ and $NiAl_2O_4$ (856–857 eV) and is different from NiO (854 eV) [45]. Recently Jun et al. reported a nickel–calcium phosphate/hydroxyapatite catalyst with the BE of Ni $2p_{3/2}$ and $2p_{1/2}$ at ca. 857 and 874 eV and with the shake-up satellite peak at ca. 862 eV. They assumed that the peak around 857 eV comes from Ni^{2+} in the phosphate (P–O–Ni–O–P) or the apatite (HO–Ni–O–P) structure [45].

An important conclusion from the ICP-OES and XPS analyses is that the chlorine content of the catalysts is negligible, and thus incorporation of $RuCl^{2+}$ species as active sites can be excluded. Using former proposals for the structure of M^{3+}-substituted HAp as analogies, Ru^{3+} may replace Ca^{2+} ions as a $Ru(OH)^{2+}$ cation [46,47]. Another possibility could be that Ru adsorbs on the surface via ion exchange with the protons of surface P–OH groups, which is similar to the structure proposed by Wakamura et al. for Cr^{3+}-exchanged HAp [35]. Note that this structure could not be confirmed by IR [35]. Furthermore, ion exchange of the
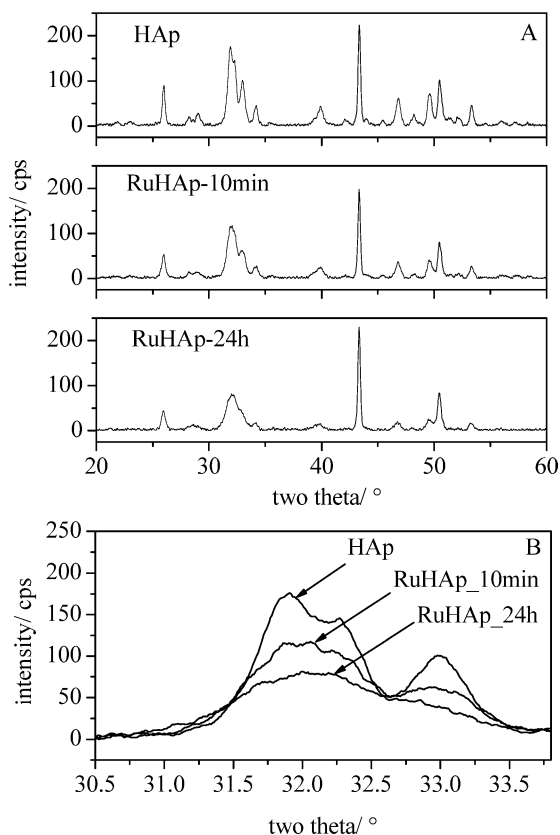
Fig. 5. XRD patterns of HAP, RuHAp-10min, and RuHAp-24h between $2\theta = 20$ and $60°$ (A), and 30.5 and $34°$ (B).

protons would give HCl and lead to a decrease in pH of the aqueous solution, contrary to the observed increase in the pH during Ru incorporation (Figs. 1 and 3).

3.3. Textural properties: BET measurement

The Ru-containing hydroxyapatite catalysts were found to be mesoporous with medium BET surface areas up to $90\ m^2\,g^{-1}$. Introduction of Ru and the promoter metal cobalt into HAp resulted in only small changes in the BET surface areas. For example, the BET surface areas (S_{BET}), micropore areas (S_t) (determined from the t-plots), and average pore diameters $\langle d \rangle$ of HAp and RuCoHAp-24h (in brackets) were as follows: S_{BET}, 81 (90) $m^2\,g^{-1}$; S_t, 10.3 (7.9) $m^2\,g^{-1}$ and $\langle d \rangle$, 20 (18) nm, respectively. Thus variations barely exceeded the estimated error of the analysis (± 5–10%).

3.4. XRD and thermal analysis

Fig. 5A compares the XRD patterns of the RuHAp catalysts prepared with different contact times. The patterns possess only diffraction peaks due to HAp. The reflexes centered at $2\theta = 43.3°$ belong to the Cu used as an internal standard. With increasing contact time between HAp and the RuCl$_3$ solution, the XRD peaks broaden (Fig. 5B), indicating that the crystallite size of the HAp phase decreases.
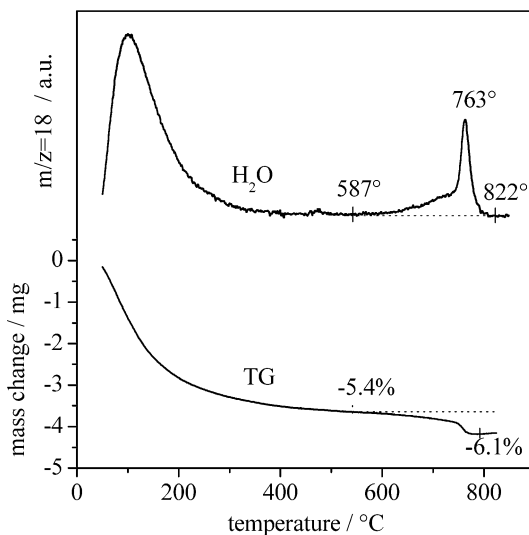
Fig. 6. Thermal analysis of RuHAp-24h (MS and TG curves).

This observation supports the importance of the dissolution–precipitation mechanism in the incorporation of Ru as discussed above.

It has been shown that the thermal stability of stoichiometric HAp (Ca/P = 1.67) is high, and it does not decompose below 1000 °C, whereas nonstoichiometric HAp (1.5 < Ca/P < 1.67) decomposes at around 700 °C into stoichiometric HAp, calcium phosphate (Ca$_3$(PO$_4$)$_2$), and H$_2$O [48]. During heat treatment the surface P–OH groups were dehydroxylated to form P–O–P connections [49]. The thermal stability of RuHAp-24h is illustrated in Fig. 6. The mass loss below 500 °C is due to desorption of water as confirmed by mass spectrometry. Decomposition of RuHAp-24h started at ca. 590 °C and ended at ca. 820 °C. XRD analysis of the sample after calcination up to 1000 °C proved the formation of Ca$_3$(PO$_4$)$_2$ via decomposition of HAp.

A comparison of the decomposition of RuHAp-10min, RuHAp-24h, and HAp is shown in Fig. 7. The observed mass losses and the mass spectrometric signals of evolved water indicate that the sample after 10 min of contact time with RuCl$_3$ behaves in a manner that is more similar to that of untreated HAp than to RuHAp-24h. The mass loss below 800 °C in HAp indicates that all three samples are nonstoichiometric, as reported by Arends et al. [48], though we used a recipe for s-HAp, and the Ca/P ratio of HAp measured by ICP-OES was the expected 1.67. RuHAp-24h decomposed distinctly differently from HAp and RuHAp-10min. The mass loss and the intensity of the $m/z = 18$ signal were much larger than those observed for HAp and RuHAp-10min. XRD analysis confirmed the observation that the amount of the decomposition product (Ca$_3$(PO$_4$)$_2$) in RuHAp-24h after thermal analysis (heating to 1000 °C) was much larger. Summing up, with increasing contact time between HAp and the RuCl$_3$ solution, the X-ray peaks became broader and the thermal stability of the materials decreased. Clearly, increasing contact time has a destabilizing effect on the apatite structure. This conclusion supports
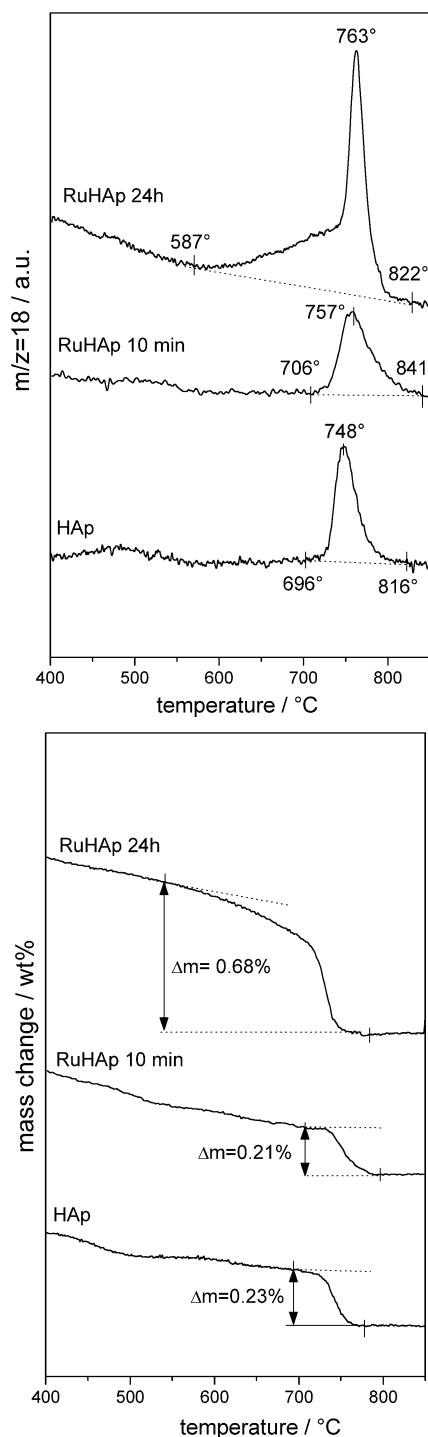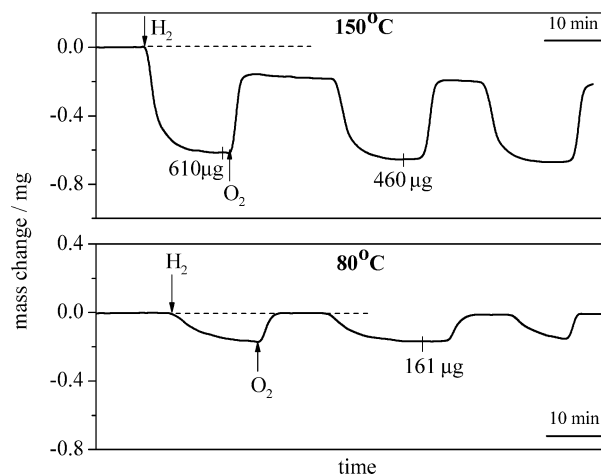
Fig. 8. Characterization of the redox behavior of RuHAp-10min with pulse thermal analysis; 73 mg catalyst, 2 ml H_2 and 1 ml O_2 pulses.

We investigated the redox behavior of RuHAp and Ru-CoHAp materials with the PulseTA technique by monitoring the mass changes resulting from the pulses of hydrogen followed by pulses of oxygen. The redox characterization of the RuHAp-10min at 80 and 150° is presented in Fig. 8. The observed mass loss due to the hydrogen pulse originated from the reduction of the catalyst only. The first reoxidation at 150 °C was not complete. The next pulses of hydrogen followed by pulses of oxygen led to the same reduction and reoxidation degree of the catalyst.

The reducibility of Ru- and Co-containing catalysts at 150 and 80 °C is compared in Fig. 9. For a short contact time (10 min) between HAp or CoHAp and the RuCl$_3$ solution the reduction degree was higher than for a long contact time (24 h), a difference that is particularly significant for the Co-containing catalysts. Interestingly, the incorporation of Co increased the redox activity of the catalysts prepared with short contact times. The reduction of RuHAp and Ru-CoHAp catalysts (Fig. 9) correlates well with the surface (Ru + Co)/Ca ratios measured by XPS (Table 2).

3.5. DRIFT spectroscopy

The infrared spectrum of HAp taken at 50 °C essentially confirmed the formation of the hydroxyapatite structure [51]. The signal at 3570 cm^{-1} is assigned to the stretching vibration of OH$^-$ ions on the lattice sites of the HAp crystals. The spectrum displayed a very broad absorption band at about 3400 cm^{-1} that, together with the signal at ca. 1630 cm^{-1}, suggests the presence of surface water molecules. Other typical bands were observed at 2138, 2074, and 2000 cm^{-1} (set of overtone and combination bands); 1093 and 1043 cm^{-1} (ν_{as}(P–O)); and 962 cm^{-1} (ν_s(P–O)). The presence of surface carbonates was indicated by the asymmetrical and symmetrical O–C–O modes found at 1547, 1491, and 1461 cm^{-1}.

Two procedures were used to investigate the different Ru-containing catalysts. According to method I the sample

Fig. 7. Comparison of the thermal stability of HAp, RuHAp-10min, and RuHAp-24h catalysts (by the TG (bottom) and MS (top) curves). The stoichiometric mass loss during the total decomposition of HAp is 1.80%.

again the importance of the dissolution–redeposition mechanism for the incorporation of Ru: the successive disappearance of the original HAp phase and the formation of a new phosphate-containing phase (or phases). Though no new phase could be detected by XRD in the samples before heat treatment, this situation is typical for the analysis of metal-exchanged apatites [50].
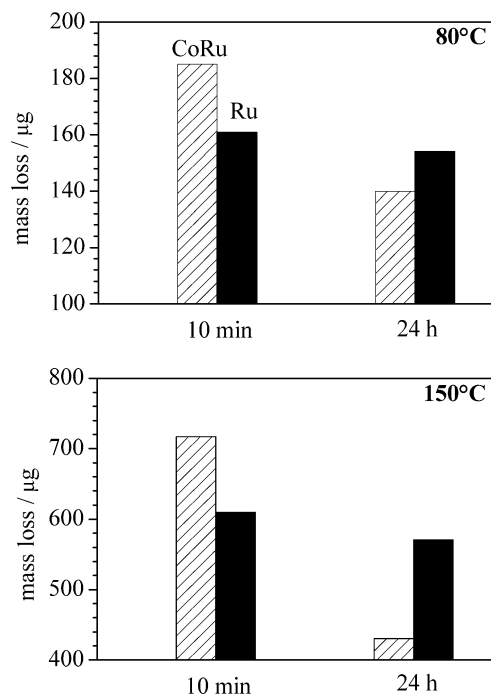
Fig. 9. Comparison of the reduction properties of the catalysts characterized by the mass loss resulting from the 2 ml hydrogen pulses at 80 and 150 °C. Black columns: RuHAp, dashed columns: RuCoHAp.

Fig. 10. (A) DRIFT spectra of (a) HAp, (b) RuHAp-10min and (c) RuCo-HAp-10min. (B) DRIFT spectra of sample RuCoHAp. The pretreatment method II was applied for both (A) and (B) (see text) and the measuring temperatures were: 50, 100, 150, 200, 250, 300° from bottom to top.

was heated under N_2 from room temperature to 300 °C at 10 °C/min, where it was kept for 2 h to remove surface water. Then the temperature was decreased to 50 °C and the sample was kept at this temperature for 30 min before heating at 6.5 °C/min to 100, 150, 200, 250, and 300 °C, always under a flow of N_2. In the other procedure (method II) no pretreatment at 300 °C was applied; the samples were stabilized only at 50 °C. In both procedures, spectra were measured at all temperatures after 30 min of equilibration time.

When the samples were pretreated according to method II, the intensity of the signal at 3570 cm^{-1} increased slightly at first and then diminished with increasing temperature (Fig. 10A). The attenuation is more evident for RuHAp and RuCoHAp than for HAp. In addition, a slight red shift to 3568 cm^{-1} was observed together with a decreasing intensity of the band of adsorbed water at 3400 cm^{-1}. Dehydration of the material occurred at these temperatures, as indicated by the decrease in the amount of adsorbed water. However, dehydration–hydration seems to be a reversible process, since spectra identical to those shown in Fig. 10A were obtained when the samples were first pretreated at 300 °C to remove water (method I). The increase in temperature and the resulting dehydration also caused a red shift in the characteristic asymmetrical and symmetrical modes of the P–O groups in the spectral region below 1100 cm^{-1}. The similar behavior of HAp, RuHAp, and RuCoHAp suggests that introduction of Ru and Co does not significantly affect the hydration–dehydration properties of hydroxyapatite.
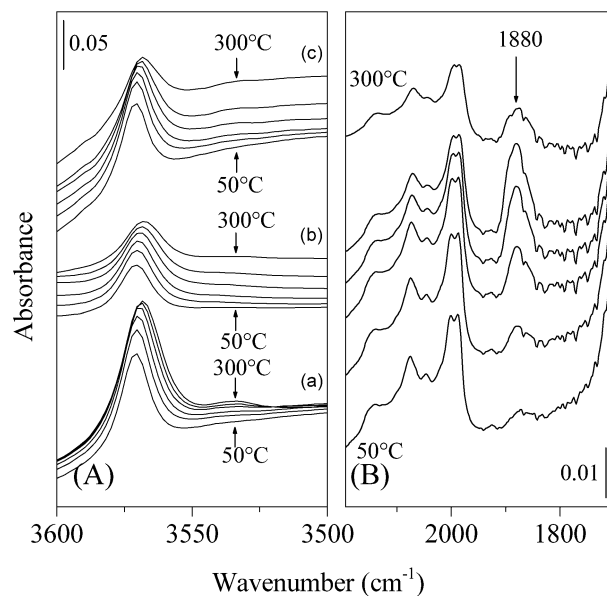
Fig. 10A shows that at 250 °C an additional band at 3535 cm^{-1} appears in the spectrum of Hap; this band is absent in the spectra of RuHAp and RuCoHAp. The intensity of the additional band in HAp increased as the temperature was raised, and the change was fully reversible. It has been suggested that the high-temperature band is the result of the reversible structural transformation of hydroxyapatite from the monoclinic to the hexagonal phase, which is in connection with an order-disorder transition in the hydroxyl columns of the hydroxyapatite structure [52]. The infrared data show that the environment of all lattice OH groups in HAp, RuHAp, and RuCoHAp samples is identical at RT. At 250 °C some of the OH groups in HAp populate a second higher energy site, whereas this disordering of the OH groups was not detectable in RuHAp and RuCoHAp.

The presence of Ru in the catalysts was confirmed by the band at 1880 cm^{-1} shown in Fig. 10B for the RuCoHAp sample. The band increased with increasing temperature for samples treated according to method II, and it was insensitive to temperature for samples pretreated at 300 °C for 2 h (method I). Moreover, the band was absent in HAp and in CoHAp at all temperatures up to 300 °C. Hence, this band reveals that an irreversible process involving Ru occurred when the sample temperature was increased to 100 °C or higher. In this respect, all Ru- and RuCo-containing samples behaved similarly.

Interpretation of the band at 1880 cm^{-1} is not straightforward. The value is too low for a Ru^{3+} carbonyl species, which is expected at 2200–2050 cm^{-1} [53]. On the other hand, bands at 1900 and 1820 cm^{-1} were observed for Ru/ZnO when the catalyst was heated in CO at 150 °C [54]. We speculate that the simultaneous coordination of carbonates and OH groups in the RuHAp and RuCoHAp samples

Table 4
The effect of contact time of Ru-incorporation into HAp and CoHAp on the catalytic activity in benzyl alcohol oxidation[a]

Catalyst (mg)	Ru content (mmol/g)	Co-content[b] (mmol/g)	Time (min)	Yield[b] (%)	TOF (h^{-1})
RuHAp-24h (38)	0.39	–	120	> 99	33
RuHAp-10min (38)	0.37	–	60	98	70
RuCoHAp-24h (50)	0.35	0.17	60	> 99	58
RuCoHAp-10min (50)	0.34	0.09	45	> 99	78

[a] Conditions: 1 mmol benzyl alcohol, 5 ml toluene, 90 °C, 1 bar O_2.
[b] The only product detectable by GC analysis was benzaldehyde.

may be connected with the appearance of this yet unobserved band at 1880 cm^{-1}.

3.6. Oxidation of benzyl alcohol: effect of catalyst pretreatment and promoters

The influence of catalyst composition and preparation conditions on the catalytic activity was investigated in the liquid-phase oxidation of benzyl alcohol, the most commonly used model compound in alcohol oxidation [1]. A preliminary study revealed that the reaction rates were distorted by the influence of mass transport in the stirred tank reactor. The likely reason for this was that the removal of the co-product water was slow, the hydrophilic catalyst adhered to the reactor wall, and the reaction rate dropped. Hence, the reaction rates expressed as turnover frequencies (TOFs) should be considered semiquantitative values; because of the mass transport effect the real reaction rates and the differences between the most and least active catalysts are greater than what the measured values indicate. In the following the activity was characterized by the TOF usually determined at close to full conversion. This average reaction rate is important for synthetic application.

A key parameter of catalyst preparation is the contact time of the RuCl$_3$ solution with HAp or CoHAp during incorporation of Ru^{3+}. The data in Table 4 show that the RuHAp and RuCoHAp catalysts prepared with a short contact time (10 min) are remarkably more active than those prepared with a long contact time (24 h). Note also the different reducibility of the Ru- and Co-containing catalysts by hydrogen (Fig. 9). Considering the continuous restructuring of the catalysts during the incorporation of Ru (Figs. 1–3, 5, and 7), the differences in oxidation and reduction activities are not astonishing. XRD analysis revealed that catalyst restructuring in the first 10 min was minor and the structure of RuHAp-10min was close to that of HAp. Thus, prolonged restructuring of the catalysts in the presence of aqueous RuCl$_3$ solution should be avoided to maximize the activity.

After the introduction of Ru into HAp or promoted HAp samples, the catalysts were washed and dried in air. We have found that the drying temperature is critical: the higher the temperature, the lower is the activity of the catalyst (Table 5). This behavior seems to be general and independent of the presence or absence of promoter (Co), the reaction temperature (90 or 60 °C), or whether initial or average re-

Table 5
Effect of pretreatment temperature on the catalytic activity in benzyl alcohol oxidation

Catalyst	Temperature (°C)	Time (min)	Conversion (%)	TOF (h^{-1})
RuHAp-24h[a]	25	152	98	26
	80	120	100	33
	110	286	98	14
	180	480	90	7.5
RuCoHAp-24h[b]	25	56	99	60
	80	60	100	58
	110	120	100	33
RuHAp-24h[c]	25	27	10	21
	80	53	10	11
	110	55	10	10
	180	120	10	5

Reaction conditions:
[a] 0.015 mmol Ru, 90 °C, 1 bar O_2, 5 ml toluene, 1 mmol benzyl alcohol.
[b] 0.0175 mmol Ru, 90 °C, 1 bar O_2, 5 ml toluene, 1 mmol benzyl alcohol.
[c] 0.021 mmol Ru, 60 °C, 1 bar O_2, 10 ml toluene, 2 mmol benzyl alcohol.

action rates are considered. A feasible explanation for the loss of activity is the dehydration of the surroundings of the active Ru species. Assuming a Ru(OH)$^{2+}$ active site, as an analogy to the structure suggested for Cr-exchanged hydroxyapatite [35], adsorbed water may stabilize the active sites in the phosphate matrix. Thermal removal of H-bonded water seems to initiate an irreversible restructuring that is detrimental to the activity. Clearly, rehydration by the co-product water during alcohol oxidation cannot regenerate the original active sites. This irreversible process could unambiguously be detected by FTIR (Fig. 10B).

To improve the catalytic activity of RuHAp, various promoter ions (Co^{2+}, Pb^{2+}, Ni^{2+}, Fe^{3+}) were introduced into the hydroxyapatite lattice before the incorporation of Ru. The effect of these ions on the oxidation activity is illustrated in Fig. 11. The two best promoters are Co and Pb. There are some examples in the literature of the positive influence of Co and Pb promoters on the performance of Ru-containing oxides and pyrochlore oxides in alcohol oxidation [55–57]. None of these catalysts, however, has high a rate and selectivity for to the carbonyl compound intermediate as RuCoHAp and RuPbHAp.

An intriguing question is the real nature of the promoter effect. Our favored explanation is the geometric effect of the modifier, that is, the active Ru species are located mainly at the surface or in the near-surface region because the pro-
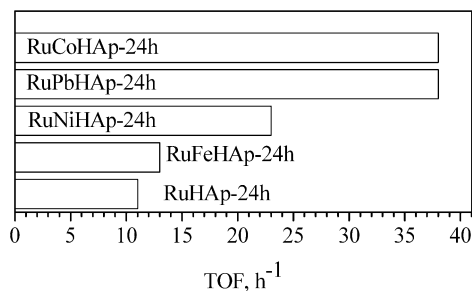
Fig. 11. Oxidation of benzyl alcohol over promoted Ru–hydroxyapatite catalysts. Reaction conditions: 0.021 mmol Ru, 10 ml toluene, 2 mmol benzyl alcohol, 60 °C, 1 bar O_2.

moter ions are already present in the solid before Ru introduction and occupy the "hidden" sites in the bulk of the catalyst particles that are inaccessible for the alcohol reactant. This explanation can best be applied for the interpretation of the outstanding activity of RuPbHAp-24h (Fig. 11). This catalyst possessed the highest surface Ru concentration, particularly when the Ru/Ca ratio is compared with that of the RuHAp-24h reference catalyst (Table 2). The assumption is not supported, however, for the other outstanding catalyst, RuCoHAp-24h.

A common interpretation for the promoting effect of Co in alcohol oxidation is an electronic interaction between Co and Ru and the resulting change in the oxidation state of Ru. Incorporation of Co into Ru-hydrotalcite increased the BE of Ru $3d_{5/2}$ from 281.7 eV to 282.7 eV; this shift was attributed to oxidation of Ru^{3+} to Ru^{4+} [55]. The higher oxidation ability of $MnFe_{1.5}Cu_{0.15}Ru_{0.35}O_4$ mixed oxide compared with that of $MnFe_{1.65}Ru_{0.35}O_4$ was explained by the lower BE of O $1s$ and the higher oxidation state of Ru [58]. In contrast, we observed a shift in the BE of Ru only in the case of RuCoHAp-24h and RNiHAp-24h, and the BE did not increase but decreased in the presence of promoter. We propose that this shift in BE may be due to changes in the environment of Ru^{3+} in the presence of Co^{2+} or Ni^{2+}.

With the average TOF as a basis for activity comparison, RuCoHAp-10min seems to be more active (TOF up to 78 h^{-1}) than other Ru-based catalysts, including the 17 wt% Ru–hydroxyapatite (2 h^{-1}) [13], Ru/Al$_2$O$_3$ (40 h^{-1}) [10], $RuO_2 \cdot xH_2O$ (1.4 h^{-1}) [9], RuO$_2$/FAU zeolite (8.7 h^{-1}) [9], Ru/CeO$_2$/CoO(OH) (10 h^{-1}) [59], Ru–Co–Al–hydrotalcite (9 h^{-1}) [55], and $[NPr_4]^+[RuO_4]^-$–SiO$_2$ (1.6 h^{-1}) [60]. All of these catalysts utilize molecular oxygen as an oxidant. A further advantage of our catalyst is the outstanding selectivity to the aldehyde intermediate: no further oxidation to carboxylic acid could be detected. In RuCoHAp the oxidation state of Co is 2+. In contrast, in Ru-Co mixed oxides cobalt exists as Co^{3+}; this species plays an essential role in the production of carboxylic acids from aldehydes via free radical pathways [57].

The RuCoHAp-10min catalyst was found to be robust without any sign of leaching, which is similar to the properties of the 17 wt% RuHAp catalyst developed by Yamaguchi et al. [13]. In our leaching test, oxidation of benzyl alcohol

was completely stopped by the removal of RuCoHAp-10min from the hot reaction solution after ca. 40% conversion, and no further conversion could be detected in the filtrate under reaction conditions.

3.7. Oxidation of various alcohols to carbonyl compounds

The influence of reactant structure on the catalyst performance was investigated with RuCoHAp-10min. This catalyst was highly active in the oxidation of various alcohols with molecular oxygen, and in all reactions shown in Table 6 the corresponding aldehyde was the only detectable product.
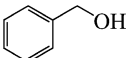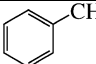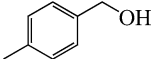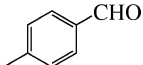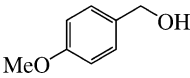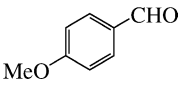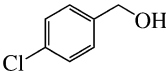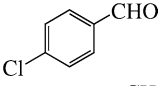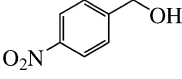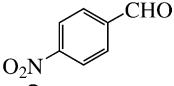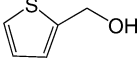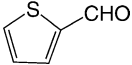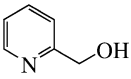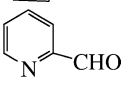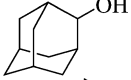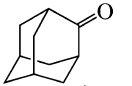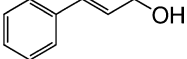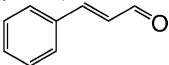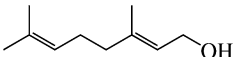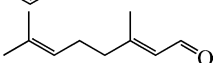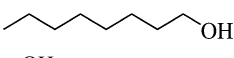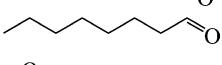
Benzylic alcohols were transformed into benzaldehydes with excellent yields. The corresponding aldehydes were obtained in high yields in the oxidation of heterocyclic alcohols 2-(hydroxymethyl)pyridine and 2-(hydroxymethyl)thiophene (Table 6, entries 6 and 7), and in the former reaction even the TOF was high (39 h^{-1}). In both reactions supported metal catalysts are poorly active [1]. Oxidation of the allylic alcohols cinnamyl alcohol (entry 9) and geraniol (entry 10) was slower than that of aromatic alcohols. Transformation of the stericall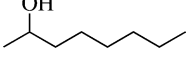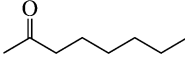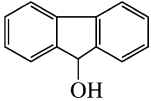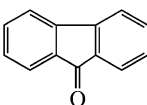y hindered secondary alcohol 2-adamantanol was relatively fast, and the ketone was obtained in high yield (entry 8). Even the oxidation of the less reactive primary aliphatic alcohol 1-octanol was reasonably fast (entry 11). Unfortunately, the catalyst deactivated after 1 h, though 68% yield was achieved without further oxidation to octanoic acid. Extended reaction times did not improve the aldehyde yield, but decreased the selectivity by successive oxidation to octanoic acid. We assume that the formation of carboxylic acid by-product is connected with the oxidation of the Co^{2+} sites of the deactivated catalyst to Co^{3+} species, which are active in aldehyde oxidation via a free radical mechanism [57]. Interestingly, the yield to the corresponding carbonyl compound was limited to about 70% also in the oxidation of 2-octanol (entry 12), though in this reaction no other product was detectable even after prolonged reaction (7 h).

Oxidation of the bulky 9-hydroxyfluorene (entry 13) ran smoothly at a TOF of 38 h^{-1}, a value that fits well in the range of TOFs achieved with other benzylic alcohols (20–78 h^{-1}). Clearly, this rigid, bulky reactant cannot migrate into the channels of HAp, demonstrating that the active sites of RuCoHAp-10min are located dominantly on the surface of the catalyst particles. In the opposite case, no activity should be observed as reported for a zeolite-confined RuO$_2$ catalyst [9].

4. Summary and conclusions

We have studied the structure and activity of promoted ruthenium–hydroxyapatite (RuXHAp) catalysts. Analysis of the processes occurring during incorporation of Ru and Co into HAp provided strong evidence for the dissolution–precipitation mechanism, though ion exchange as a compet-

Table 6
Oxidation of various alcohols with RuCoHAp and molecular oxygen[a]

Entry	Reactant	Product	Time (h)	Yield[c] (%)	TOF[d] (h^{-1})
1			0.75	> 99	78
2			0.75	> 99	78
3			1.25	> 99	47
4			0.75	> 99	78
5			3	98	20
6			1.5	> 99	39
7[b]			8	94	3.5
8			4	97	14
9[b]			2.5	> 99	12
10[b]			2	73	11
11[b]			1	68	20
12[b]			2	72	11
13			0.75	48	38

[a] 0.05 g RuCoHAp-10min (Ru, 0.34 mmol/g), 1 mmol alcohol, 5 ml toluene, 1 bar O_2, 90 °C.
[b] 0.1 g RuCoHAp-10min.
[c] Selectivity always 100%.
[d] Average turnover frequency, related to the total amount of Ru^{3+}.

ing mechanism could not be excluded. Note that there is a lively debate even in the recent literature on the importance of these two processes in the evolution of metal-exchanged hydroxyapatites [19,61].

ICP-OES, XPS, XRD, and thermal analysis proved that the catalysts obtained after short (10 min) or long (24 h) contact times between the $RuCl_3$ solution and HAp or CoHAp have different compositions due to a continuous restructuring and formation of a new solid phase or phases. The extent of restructuring depends on the experimental conditions, including the Ru concentration and the presence of promoter ions in solution and the pH. The considerable surface enrichment of Ru observed with all catalysts (Table 2) indicates an "eggshell"-type structure that is important for minimizing mass transport limitation inside the catalyst particles. The rapid oxidation of 9-hydroxyfluorene (Table 6) confirmed that the active ruthenium species are located dominantly

on the surface of the catalyst particles. The reducibility of RuHAp and RuCoHAp catalysts determined by hydrogen pulses in thermal analysis (Fig. 9) correlated well with the surface (Ru + Co)/Ca ratios measured by XPS (Table 2).

The higher activity of promoted Ru catalysts, particularly that of RuPbHAp, is probably due to the steric effect of promoter that occupies those sites that are poorly accessible for the reactant during oxidation. The variations in the binding energy of Ru due to promotion by Co or Ni (Table 3) are attributed to the different coordination environment of Ru^{3+} ions. The Cl^- content of the catalysts was negligible, and Ru seems to be present as isolated Ru^{3+} ions, possibly as $Ru(OH)^{2+}$ species to compensate for the charge imbalance when Ca^{2+} ions are substituted [27,35].

The promoted ruthenium–hydroxyapatite catalysts RuCoHAp and RuPbHAp are easy to prepare and robust and can be used under mild conditions without any sign of leach-

ing of the active species. To optimize the catalyst structure and the location of the active species, it is important to apply a relatively low $RuCl_3$ concentration and a short contact time during the incorporation of Ru. Heat treatment of the catalyst after incorporation of Ru is also detrimental because of dehydration and irreversible restructuring of the active species and its surroundings.

The appropriately prepared Co- or Pb-promoted catalysts are highly efficient in the oxidation of various activated and nonactivated alcohols to the corresponding carbonyl compounds with molecular oxygen. Gas chromatographic analysis could not detect further oxidation of aldehydes to carboxylic acids, except in the oxidation of a primary aliphatic alcohol under forcing conditions. The activity of RuCoHAp-10min, expressed as average TOF at high conversion, surpasses those of other catalysts possessing Ru as active species, such as supported metallic Ru or Ru complexes, and ruthenium oxide and mixed oxides [9,10,57].

Considering the results from a broader perspective, we can conclude that the activity of promoted RuHAp catalysts is inferior to those of supported platinum and palladium [1]. None of these supported metal catalysts, however, offer selectivities in the oxidation of primary alcohols to aldehydes as excellent as those of RuCoHAp and RuPbHAp. In the synthesis of structurally complex and expensive aldehydes, such as fine chemicals and pharmaceutical intermediates, high yield is the critical requirement, not the short reaction time, and in this field our promoted RuHAp catalysts may be the preferred choice.

References

[1] T. Mallat, A. Baiker, Chem. Rev. 104 (2004) 3037.
[2] M. Besson, P. Gallezot, Catal. Today 57 (2000) 127.
[3] T. Nishimura, S. Uemura, Catal. Surveys Jpn. 4 (2000) 135.
[4] S. Biella, G.L. Castiglioni, C. Fumagalli, L. Prati, M. Rossi, Catal. Today 72 (2002) 43.
[5] J. Muzart, Tetrahedron 59 (2003) 5789.
[6] R. Anderson, K. Griffin, P. Johnston, P.L. Alsters, Adv. Synth. Catal. 345 (2003) 517.
[7] T. Naota, H. Takaya, S.I. Murahashi, Chem. Rev. 98 (1998) 2599.
[8] M. Matsumoto, N. Watanabe, J. Org. Chem. 49 (1984) 3435.
[9] B.Z. Zhan, M.A. White, T.K. Sham, J.A. Pincock, R.J. Doucet, K.V.R. Rao, K.N. Robertson, T.S. Cameron, J. Am. Chem. Soc. 125 (2003) 2195.
[10] K. Yamaguchi, N. Mizuno, Angew. Chem., Int. Ed. 41 (2002) 4538.
[11] K. Kaneda, T. Yamashita, T. Matsushita, K. Ebitani, J. Org. Chem. 63 (1998) 1750.
[12] K. Yamaguchi, N. Mizuno, New J. Chem. 26 (2002) 972.
[13] K. Yamaguchi, K. Mori, T. Mizugaki, K. Ebitani, K. Kaneda, J. Am. Chem. Soc. 122 (2000) 7144.
[14] L. Calderin, M.J. Stott, A. Rubio, Phys. Rev. B 67 (2003) 134106.
[15] T. Kanazawa, in: Inorganic Phosphate Materials, Elsevier, Amsterdam, 1989, pp. 15–54.
[16] M.J. Kohn, J. Rakovan, J.M. Hughes, Phosphates: Geochemical, Geobiological and Materials Importance, in: Reviews in Mineralogy and Geochemistry, vol. 48, Mineralogical Society of America, 2002, pp. 1–49.
[17] J.C. Eliott, Structure and Chemistry of the Apatites and Other Calcium Orthophosphates, Elsevier, Amsterdam, 1994.
[18] J. Guerra-Lopez, R. Pomes, C.O. Della Vedova, R. Vina, G. Punte, J. Raman Spectrosc. 32 (2001) 255.
[19] E. Valsami-Jones, K.V. Ragnarsdottir, A. Putnis, D. Bosbach, A.J. Kemp, G. Cressey, Chem. Geol. 151 (1998) 215.
[20] S. Sugiyama, T. Shono, D. Makino, T. Moriga, H. Hayashi, J. Catal. 214 (2003) 8.
[21] S. Sugiyama, T. Shono, E. Nitta, H. Hayashi, Appl. Catal. A 211 (2001) 123.
[22] K. Elkabouss, M. Kacimi, M. Ziyad, S. Ammar, F. Bozon-Verduraz, J. Catal. 226 (2004) 16.
[23] T. Hara, K. Mori, T. Mizugaki, K. Ebitani, K. Kaneda, Tetrahedron Lett. 44 (2003) 6207.
[24] S. Sugiyama, J.B. Moffat, Catal. Lett. 76 (2001) 75.
[25] U.R. Pillai, E. Sahle-Demessie, Appl. Catal. A 261 (2004) 69.
[26] M. Murata, T. Hara, K. Mori, M. Ooe, T. Mizugaki, K. Ebitani, K. Kaneda, Tetrahedron Lett. 44 (2003) 4981.
[27] S. Wuyts, D.E. De Vos, F. Verpoort, D. Depla, R. De Gryse, P.A. Jacobs, J. Catal. 219 (2003) 417.
[28] A. Smahi, A. Solhy, H. El Badaoui, A. Amoukal, A. Tikad, M. Maizi, S. Sebti, Appl. Catal. A 250 (2003) 151.
[29] K. Mori, T. Hara, T. Mizugaki, K. Ebitani, K. Kaneda, J. Am. Chem. Soc. 125 (2003) 11460.
[30] S. Sugiyama, T. Minami, H. Hayashi, M. Tanaka, N. Shigemoto, J.B. Moffat, J. Chem. Soc., Faraday Trans. 92 (1996) 293.
[31] M. Maciejewski, C.A. Muller, R. Tschan, W.D. Emmerich, A. Baiker, Thermochim. Acta 295 (1997) 167.
[32] J.D. Grunwaldt, M.D. Wildberger, T. Mallat, A. Baiker, J. Catal. 177 (1998) 53.
[33] C.D. Wagner, L.E. Davis, M.V. Zeller, J.A. Taylor, R.H. Raymond, L.H. Gale, Surf. Interface Anal. 3 (1981) 211.
[34] M. Goethals, B. Vanderstraeten, J. Berghmans, G. De Smedt, S. Vliegen, E. Van't Oost, J. Hazard. Mater. A 70 (1999) 93.
[35] M. Wakamura, K. Kandori, T. Ishikawa, Colloid Surf. A 142 (1998) 107.
[36] Y.P. Xu, F.W. Schwartz, S.J. Traina, Environ. Sci. Technol. 28 (1994) 1472.
[37] Q.Y. Ma, S.J. Traina, T.J. Logan, J.A. Ryan, Environ. Sci. Technol. 27 (1993) 1803.
[38] A. Yasukawa, T. Yokoyama, K. Kandori, T. Ishikawa, Colloid Surf. A 238 (2004) 133.
[39] K.S. Kim, N. Winograd, J. Catal. 35 (1974) 66.
[40] T. Ishikawa, H. Saito, A. Yasukawa, K. Kandori, Bull. Chem. Soc. Jpn. 69 (1996) 899.
[41] N.S. McIntyre, M.G. Cook, Anal. Chem. 47 (1975) 2208.
[42] M. Oku, K. Hirokawa, J. Electron Spectrosc. Relat. Phenom. 8 (1976) 475.
[43] V.I. Nefedov, Y.V. Salyn, P.M. Solozhenkin, G.Y. Pulatov, Surf. Interface Anal. 2 (1980) 170.
[44] V.I. Nefedov, Y.V. Salyn, K. Keller, Zhurnal Neorg. Khimii 24 (1979) 2564.
[45] J.H. Jun, T.J. Lee, T.H. Lim, S.W. Nam, S.A. Hong, K.J. Yoon, J. Catal. 221 (2004) 178.
[46] M. Wakamura, K. Kandori, T. Ishikawa, Colloid Surf. A 164 (2000) 297.
[47] T. Ishikawa, Stud. Surf. Sci. Catal. 99 (1996) 301.
[48] J. Arends, J. Christoffersen, M.R. Christoffersen, H. Eckert, B.O. Fowler, J.C. Heughebaert, G.H. Nancollas, J.P. Yesinowski, S.J. Zawacki, J. Cryst. Growth 84 (1987) 515.
[49] H. Tanaka, M. Chikazawa, K. Kandori, T. Ishikawa, Phys. Chem. Chem. Phys. 2 (2000) 2647.
[50] A. Bigi, G. Falini, E. Foresti, M. Gazzano, A. Ripamonti, N. Roveri, J. Inorg. Biochem. 49 (1993) 69.
[51] S. Koutsopoulos, J. Biomed. Mater. Res. 62 (2002) 600.
[52] I. Reisner, W.E. Klee, Spectrochim. Acta, Part A 38 (1982) 899.
[53] K.I. Hadjiivanov, G.N. Vayssilov, Adv. Catal. 47 (2002) 307.
[54] E. Guglielminotti, F. Boccuzzi, Surf. Sci. Catal. 48 (1989).
[55] T. Matsushita, K. Ebitani, K. Kaneda, Chem. Commun. (1999) 265.

[56] T.R. Felthouse, P.B. Fraundorf, R.M. Friedman, C.L. Schosser, J. Catal. 127 (1991) 393.

[57] M. Musawir, P.N. Davey, G. Kelly, I.V. Kozhevnikov, Chem. Commun. (2003) 1414.

[58] H.B. Ji, K. Ebitani, T. Mizugaki, K. Kaneda, Catal. Commun. 3 (2002) 511.

[59] K. Ebitani, H.B. Ji, T. Mizugaki, K. Kaneda, J. Mol. Catal. A 212 (2004) 161.

[60] R. Ciriminna, S. Campestrini, M. Pagliaro, Adv. Synth. Catal. 346 (2004) 231.

[61] S. Sugiyama, N. Fukuda, H. Matsumoto, H. Hayashi, N. Shigemoto, Y. Hiraga, J.B. Moffat, J. Colloid Interface Sci. 220 (1999) 324.